Perovskite as a spin current generator

Makoto Naka,[1] Yukitoshi Motome,[2] and Hitoshi Seo[3,4]
[1]*Waseda Institute for Advanced Study, Waseda University, Shinjuku, Tokyo 169-8050, Japan*
[2]*Department of Applied Physics, The University of Tokyo, Bunkyo, Tokyo 113-8656, Japan*
[3]*Condensed Matter Theory Laboratory, RIKEN, Wako, Saitama 351-0198, Japan*
[4]*Center for Emergent Matter Science, RIKEN, Wako, Saitama 351-0198, Japan*

(Received 19 November 2020; revised 2 February 2021; accepted 22 February 2021; published 5 March 2021)

We theoretically show that materials with perovskite-type crystal structures provide a platform for spin current generation. Its mechanism is based on spin-split band structures in certain kinds of collinear antiferromagnetic states, requiring neither spin-orbit coupling nor a ferromagnetic moment. By investigating a multiband Hubbard model for transition-metal compounds by means of the Hartree-Fock approximation and the Boltzmann transport theory, we find that a pure spin current is induced by an electric field applied to a C-type antiferromagnetic metallic phase. The spin current generation originates from a cooperative effect of spatially anisotropic electron transfer integrals owing to the $GdFeO_3$-type lattice distortion, which is ubiquitous in many perovskites, and the collinear spin configuration. We discuss our finding from the symmetry point of view, in comparison with other spin current generator candidates with collinear antiferromagnetism. We also propose several ways to detect the phenomenon in candidate perovskite materials.

DOI: 10.1103/PhysRevB.103.125114

I. INTRODUCTON

Perovskites, a large family of compounds with the chemical formula ABX_3 as the mother phase and their related structures, show versatile functionalities and serve as one of the most well-studied textbook materials in condensed-matter physics [1–4]. In particular, transition-metal-based perovskites exhibit a wide range of properties, e.g., ferroelectricity, metal-to-insulator (MI) transition, the magnetoelectric effect, the spin crossover phenomenon, superconductivity, and the photovoltaic effect [5–10]. The diverse physical properties are created by chemical substitutions which control the electronic states by tuning their band filling, bandwidth, and dimensionality. Amazingly, the rich variety originates from a common framework of d electrons of the transition-metal (TM) elements B and p electrons of the ligands X. Here, we show that yet another functionality can be extracted which has been overlooked for decades: spin current generation useful for spintronic devices.

In the field of spintronics, the search for materials for efficiently generating spin currents has been pursued, which has not been limited to conventionally used ferrimagnets and ferromagnets [11–15]. Semiconductors and metals with heavy elements have been considered as candidates by the realization of the spin Hall effect [16–22], whose mechanism relies on the spin-orbit coupling. Recently, the search has been extended to antiferromagnets with noncollinear [23,24] and collinear magnetic structures [25–29]. For future applications, exploring such functionality in a feasible way using ubiquitous materials is crucial.

In this paper, we theoretically propose that perovskite TM compounds work as an efficient spin current generator. Adopting a multiorbital Hubbard model for the d orbitals of the TM ions, we investigate spin transport properties in an applied electric field. A key ingredient is the so-called $GdFeO_3$-type lattice distortion [30,31], commonly seen in the ABX_3 compounds and known to control the bandwidth via the tolerance factor, a ratio between the ionic radii of three elements. The distorted perovskite structure is shown in Fig. 1(a), in which the regularly aligned BX_6 octahedra on the cubic lattice rotate to fill the crystal voids around the A sites, as illustrated in Fig. 1(b) (see below). Consequently, the symmetry of the crystal structure is lowered to an orthorhombic *Pnma* space group. We will show that the spin current conductivity becomes nonzero in a metallic state with the C-type AFM (C-AFM) ordering illustrated in Fig. 1(c) and increases with the $GdFeO_3$-type distortion. The spin current generation here originates from the spin splitting of the energy band in the C-AFM state due to the spatial anisotropies of the transfer integrals arising from the $GdFeO_3$-type distortion. We discuss the symmetry aspect of the spin current generation in comparison with previous studies for collinear antiferromagnets. Finally, we propose how to verify our proposal by presenting candidate perovskite TM compounds.

II. MODEL AND METHOD

Let us introduce how to incorporate the $GdFeO_3$-type distortion for modeling ABX_3. We start with the tight-binding d-p model composed of the five d orbitals of the TM ions with cubic crystalline field splitting together with the three p orbitals of the ligands [32–34]. The $GdFeO_3$-type distortion is characterized by two kinds of rotation modes of the BX_6 octahedra [31]: a major rotation $\pm\phi$ around the [110] or [$\bar{1}$10] axis, followed by an additional tilting $\psi = \pm\arctan[\sqrt{2}(1-\cos\phi)/(2+\cos\phi)]$ around the [001] axis [see Fig. 1(b)].

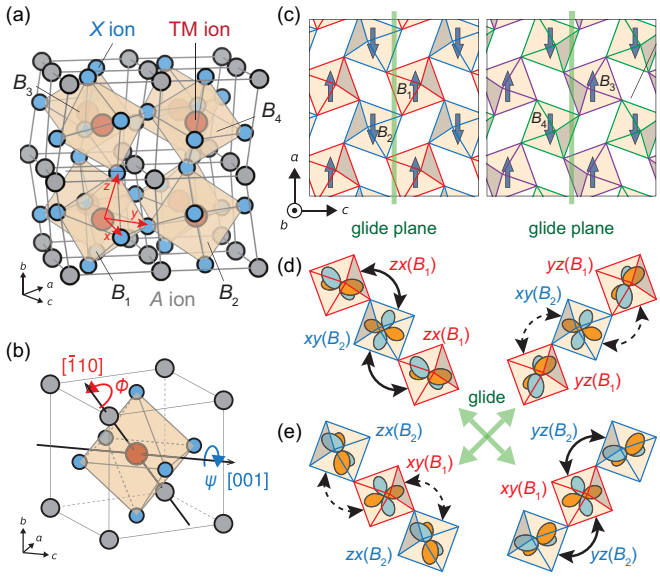

FIG. 1. (a) Perovskite structure with the $GdFeO_3$-type distortion. B_1–B_4 denote the BX_6 octahedra contained in the unit cell, connected by symmetry operations and thus crystallographically equivalent. The *abc* axes are defined for the *Pnma* space group. The *xyz* axes represent the local coordinate defined for each octahedron. (b) Two kinds of BX_6 rotation modes of the $GdFeO_3$-type distortion described in the text. (c) Schematic illustration of the *C*-type AFM spin configuration in the two *ac* planes. The blue arrows represent up- and down-spin moments of the *d* orbitals in the TM ions. The green lines denote the glide plane perpendicular to the *ac* plane. Schematic illustrations of the anisotropies of the t_{2g}-t_{2g} transfer integrals on (d) B_1-B_2-B_1 and (e) B_2-B_1-B_2 bonds along the [101] and [10$\bar{1}$] directions. The magnitudes of the transfer integrals denoted by the solid arrows are larger than those denoted by the dashed arrows in the presence of the distortion.

Here, we adopt an effective tight-binding model for the *d* orbitals derived by the second-order perturbation in terms of the *d*-*p* electron transfer integrals [3,33], which is given by

$$\mathcal{H}_0 = \sum_{i\beta\sigma} \epsilon_\beta n_{i\beta\sigma} + \sum_{ij\beta\beta'\sigma} \left[\hat{t}^{dd}_{ij}(\phi)\right]_{\beta\beta'} c^\dagger_{i\beta\sigma} c_{j\beta'\sigma}, \qquad (1)$$

where $c_{i\beta\sigma}$ and $n_{i\beta\sigma}$ $(= c^\dagger_{i\beta\sigma} c_{i\beta\sigma})$ are the annihilation and number operators of an electron with spin σ of the *d* orbital β $(= x^2-y^2, 3z^2-r^2, xy, yz, zx)$, respectively, represented in the local *xyz* axes fixed on the *i*th octahedron shown in Fig. 1(a), and the spin axes are globally defined for all the sites. We assume that the energy levels of the *d* orbitals are given as $\epsilon_{x^2-y^2} = \epsilon_{3z^2-r^2} = 3\Delta_{\rm cf}/5$ and $\epsilon_{xy} = \epsilon_{yz} = \epsilon_{zx} = -2\Delta_{\rm cf}/5$ with the octahedral crystalline field splitting $\Delta_{\rm cf}$ between the e_g and t_{2g} manifolds. We consider the nearest-neighbor *d*-*d* transfer integral, given by

$$\left[\hat{t}^{dd}_{ij}(\phi)\right]_{\beta\beta'} = -\frac{1}{\Delta_{\rm ct}} \sum_{\gamma\gamma'} \left[\hat{t}^{pd}_{i;ij}\right]^\top_{\beta\gamma} \left[\hat{\mathcal{R}}_{ij}(\phi)\right]_{\gamma\gamma'} \left[\hat{t}^{pd}_{j;ij}\right]_{\gamma'\beta'}, \qquad (2)$$

where $\Delta_{\rm ct}$ is the charge transfer energy between the *p* and *d* orbitals. $\hat{t}^{pd}_{i;ij}$ is the 3×5 transfer integral matrix from the *d* orbitals of the *i*th TM ion to the *p* orbitals of the ligand shared by the *i*th and *j*th octahedra defined in the coordinate for the *i*th octahedron; $\hat{t}^{pd}_{i;ij}$ is given by the Slater-Koster parameters $V_{pd\sigma}$ and $V_{pd\pi}$ [35]. $\hat{\mathcal{R}}_{ij}(\phi)$ is the 3×3 matrix defined by $\hat{\mathcal{R}}_{ij}(\phi) = \hat{R}^\top_i(\phi)\hat{R}_j(\phi)$, where $\hat{R}_i(\phi)$ represents the rotation of the *i*th octahedron.

An important feature of the resultant *d*-*d* transfer integrals is their spatial anisotropy depending on the bond directions, owing to the hybridization between the different *d* orbitals induced by the BX_6 rotations. The *d* sites are divided into four kinds of sites termed B_1–B_4 in the unit cell; B_1 and B_2, B_3 and B_4 are respectively connected by the glide symmetry [the glide plane is drawn in Fig. 1(c)]. As shown in Fig. 1(d), for example, the transfer integral between the *zx* orbital in B_1 [$zx(B_1)$] and the *xy* orbital in B_2 [$xy(B_2)$] in the [10$\bar{1}$] direction becomes nonzero, which is zero in the cubic structure without $GdFeO_3$-type distortion since the orbitals are orthogonal to each other, and is larger than that between the $yz(B_1)$ and $xy(B_2)$ orbitals in the [101] direction. On the other hand, on the B_2-B_1-B_2 bonds, the magnitudes of the electron transfers in the [101] and [10$\bar{1}$] directions are switched with each other as shown in Fig. 1(e), reflecting the glide symmetry which connects the B_1 and B_2 sites. They yield the anisotropic transfer integrals depending on the bond directions within the *ac* plane. Here, we note that the hopping integrals between the *d* orbitals connected by the glide operation, e.g., $xy(B_1)$ and $xy(B_2)$, and $yz(B_1)$ and $zx(B_2)$, are isotropic in the *ac* plane, even in the presence of the $GdFeO_3$-type distortion [36].

The on-site Coulomb interactions between the *d* electrons are introduced in the conventional manner as

$$\begin{aligned}\mathcal{H}_{\rm int} = {} & U \sum_{i\beta} n_{i\beta\uparrow} n_{i\beta\downarrow} + \frac{U'}{2} \sum_{i\beta\neq\beta'} n_{i\beta} n_{i\beta'} \\ & + J \sum_{i\beta>\beta'\sigma\sigma'} c^\dagger_{i\beta\sigma} c^\dagger_{i\beta'\sigma'} c_{i\beta\sigma'} c_{i\beta'\sigma} \\ & + I \sum_{i\beta\neq\beta'} c^\dagger_{i\beta\uparrow} c^\dagger_{i\beta\downarrow} c_{i\beta'\downarrow} c_{i\beta'\uparrow}, \end{aligned} \qquad (3)$$

where U and U' represent the intra and interorbital Coulomb interactions, respectively, J is Hund's coupling, and I is the pair hopping interaction. Here, we do not take into account the spin-orbit coupling, which is not essential for the present mechanism.

We analyze the effective five-orbital Hubbard model defined by $\mathcal{H} = \mathcal{H}_0 + \mathcal{H}_{\rm int}$ within the Hartree-Fock approximation, where the mean fields $\langle c^\dagger_{i\beta\sigma} c_{i\beta'\sigma}\rangle$ are self-consistently determined. Using the Hartree-Fock eigenenergies and eigenstates, the conductivity of the spin current with the spin parallel to the AFM moment along the μ axis with respect to an electric field parallel to the ν axis is computed by means of the Boltzmann transport theory with the relaxation-time approximation as

$$\chi_{\mu\nu} = \frac{-e\tau}{2NV} \sum_{\boldsymbol{k}m\sigma} \sigma v^\mu_{\boldsymbol{k}m\sigma} v^\nu_{\boldsymbol{k}m\sigma} \left[-\frac{\partial f(\epsilon_{\boldsymbol{k}m\sigma})}{\partial \epsilon_{\boldsymbol{k}m\sigma}}\right], \qquad (4)$$

where $f(\epsilon_{\boldsymbol{k}m\sigma})$ is the Fermi distribution function for the Bloch eigenstate with the wave vector $\boldsymbol{k}$, the band index m, and the spin $\sigma(=\pm 1)$. $v^\mu_{\boldsymbol{k}m\sigma}$ is the μ component of the group velocity of the wave packet centered on the state $|\boldsymbol{k}m\sigma\rangle$, τ is the transport relaxation time, V is the volume of the unit

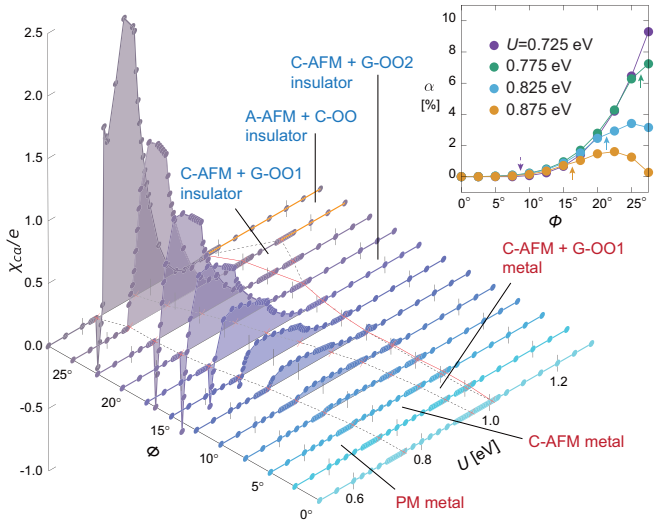

FIG. 2. Spin current conductivity χ_{ca} on the U-ϕ plane. The black dashed lines on the basal plane indicate the phase boundaries between the different phases. The red solid line stands for the MI transition. The thick orange line represents the region where the A-AFM + C-OO phase is stable. The inset shows the ϕ dependences of the charge-spin current conversion rate α in the C-AFM metallic phases. The dashed and solid arrows indicate the phase boundaries between the PM and C-AFM phases and between the C-AFM and C-AFM + G-OO1 phases, respectively.

cell, and N is the total number of unit cells. Note that the spin current is conserved in the present model without spin-orbit coupling. The calculation by Eq. (4) is equivalent to that by the linear response theory based on the Kubo formula when the relaxation time τ is long enough [27].

In the following calculation, we choose model parameters typical of perovskite $3d$ TM oxides: $V_{pd\sigma} = 2$ eV, $V_{pd\pi} = 1$ eV, $\Delta_{\rm cf} = 3$ eV, and $\Delta_{\rm ct} = 5$ eV [32]. As for the Coulomb interaction terms, we adopt the relations $U = U' + 2J$ and $J = I$ [37]. While the model is known to exhibit a variety of spin and orbital orders depending on the electron filling n (the electron number per site on average) and other parameters [32], we find that the C-AFM order can make an off-diagonal component of the spin current conductivity, χ_{ca}, nonzero; hence, below we show the results for $n = 2$, where the C-AFM order was obtained under electron correlations and the $GdFeO_3$-type distortion [32] by changing U and the rotation angle of the BX_6 octahedra ϕ, while keeping the ratios $U' = 2U/3$ and $J = U/6$. We note that χ_{ca} becomes nonzero under the C-AFM order irrespective of n. The $\boldsymbol{k}$-space mesh, equivalent to N, is chosen to be 16×10^3 and 10^6 to evaluate the mean fields and the spin current conductivity, respectively. We set the relaxation time as $1/\tau = 1$ meV and the lattice constants to unity.

III. RESULTS

Figure 2 shows the off-diagonal spin current conductivity χ_{ca} as a function of U and ϕ, together with the phase diagram on the basal plane. In the absence of the $GdFeO_3$-type distortion ($\phi = 0$), when U is increased from the paramagnetic (PM) metallic phase, a phase transition to the C-AFM metallic phase occurs at $U \simeq 0.75$ eV. By increasing U further, two kinds of G-type orbital ordering (G-OO1 for $0.95 \lesssim U \lesssim 1.01$ eV and G-OO2 for $U \gtrsim 1.01$ eV) are stabilized, coexisting with the C-AFM order. In the two orbital ordered phases, nearly one electron commonly occupies the xy orbital at each site, and the other electrons alternately occupy $\frac{1}{\sqrt{2}}(yz + zx)$ and $\frac{1}{\sqrt{2}}(yz - zx)$ in G-OO1, while they occupy zx and yz in G-OO2 [32]. Near the phase transition between the G-OO1 and G-OO2 phases, the system undergoes a MI transition. These C-AFM phases are robust against the introduction of ϕ except at $\phi \gtrsim 25^\circ$ in the large-U region, where the A-type AFM (A-AFM) phase accompanied by the C-type orbital order (C-OO) of the yz and zx orbitals is stabilized instead.

As shown in Fig. 2, χ_{ca} is constantly zero at $\phi = 0$, irrespective of the value of U, while it becomes nonzero in the presence of the $GdFeO_3$-type distortion in the C-AFM metallic phases. This means that in this region a charge current along the a axis is converted into a spin current along the c axis. We note that the conductivity tensor is symmetric, $\chi_{ca} = \chi_{ac}$, with vanishing diagonal elements, $\chi_{aa} = \chi_{cc} = 0$. The inset in Fig. 2 shows the ϕ dependences of the charge-spin current conversion rate defined by $\alpha \equiv (2e/\hbar)(\chi_{ca}/\sigma_{aa})$ with the electrical conductivity σ_{aa} calculated within the same scheme [23,25]. α basically increases with ϕ up to around 6% at $\phi = 25^\circ$ in the C-AFM metallic phase, which is comparable to that observed in Pt originating from the spin Hall effect due to the strong spin-orbit coupling [38].

Let us investigate the microscopic mechanism of the off-diagonal spin current response. First, we show the energy band structure in the C-AFM phase at $(U, \phi) = (0.775\ \text{eV},\ 25^\circ)$, where the Fermi energy resides in the t_{2g} bands. Figure 3(a) shows the up- and down-spin electron bands along the symmetry lines illustrated in the inset. A spin splitting appears in the general $\boldsymbol{k}$ points except for the planes $k_c = 0, \pm 0.5$ and $k_a = 0, \pm 0.5$ in the Brillouin zone. This is a consequence of the glide symmetry breaking by the collinear AFM order (note that the spin-orbit coupling is absent in our model and the glide operation considered here does not act on the spins), as similarly discussed in different systems [25–27,29].

Next, we show the up- and down-spin Fermi surfaces in Figs. 3(b) and 3(c), respectively, together with the group velocities $\boldsymbol{v}_{km\sigma}$ along them. We show the results at $k_b = 0.39$ since the Fermi surfaces reside near $k_b \simeq 0.5$ [see Fig. 3(a)]. The up-spin Fermi surfaces are mainly composed of the one-dimensional-like curves along the [101] direction and the two-dimensional rhombi. There, the group velocities are relatively large on the parts of the Fermi surfaces parallel to the [101] direction. These features imply that, when an electric field is applied along the [100] direction, the up-spin electrons drift to the $[\bar{1}01]$ direction. On the other hand, the down-spin Fermi surfaces, which correspond to the mirror images of the up-spin ones with respect to the k_a-k_b plane, carry the down-spin electrons along the $[\bar{1}0\bar{1}]$ direction under the [100] electric field. As a result of this spin-dependent anisotropy, the spin current flows along the [001] direction perpendicular to the electric field.

Furthermore, we can pin down the d-orbital component most responsible for the spin-dependent transport. Figures 3(d) and 3(e) show the relative weights of the t_{2g} orbitals

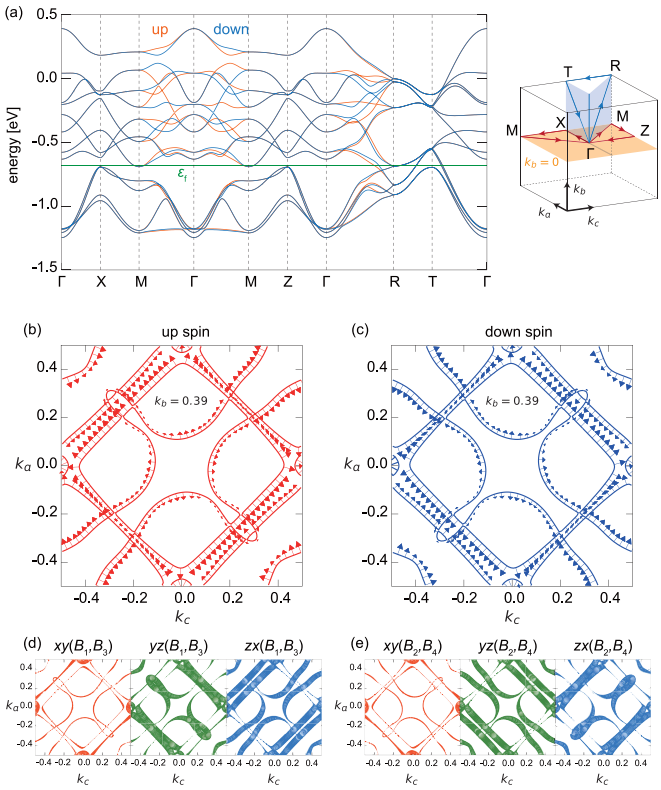

FIG. 3. (a) Energy band structure in the C-AFM metallic phase at $(U, \phi) = (0.725\ \text{eV}, 25^\circ)$. The Fermi energy is denoted by ε_f. The right panel shows the symmetry lines in the first Brillouin zone. (b) and (c) The group velocities of the up- and down-spin electrons, respectively, on the Fermi surfaces at $k_b = 0.39$. k_c and k_a stand for the coefficients of the reciprocal vectors $\boldsymbol{b}_c$ and $\boldsymbol{b}_a$, respectively. The length of the red and blue arrows represents the magnitude of the group velocity on each $\boldsymbol{k}$ point. (d) and (e) are the relative weights of the t_{2g} orbitals on the up- and down-spin Fermi surfaces, respectively. The areas of the red, green, and blue circles represent the magnitudes of the xy (left), yz (middle), and zx (right) components on (b) (B_1, B_3) and (c) (B_2, B_4) sublattices.

on the (B_1, B_3) sublattice in the up-spin Fermi surfaces and those on the (B_2, B_4) sublattice in the down-spin Fermi surfaces, respectively; the other components are smaller and therefore are not shown. The zx (yz) orbitals on the B_1 (B_2) and B_3 (B_4) sites, where the majority spin is up (down), compose the Fermi surfaces parallel to the [101] ($[\bar{1}01]$) direction, as mentioned above, dominating the anisotropic spin transport. These features are indeed consistent with the real-space anisotropic transfer integrals due to the $GdFeO_3$-type distortion shown in Figs. 1(d) and 1(e); the up(down)-spin electrons on the B_1 (B_2) sites tend to hop in the $[\bar{1}01]$ ([101]) direction, having a larger transfer integral than the [101] ($[\bar{1}01]$) direction.

IV. DISCUSSION

A similar anisotropic spin transport owing to the combination of a collinear AFM spin structure and site-dependent anisotropic transfer integrals was proposed for quasi-two-dimensional κ-type organic conductors [25]. In that case molecular dimers have two different orientations, leading to dimer-dependent anisotropic transfer integrals. From the viewpoint of crystalline symmetry, the present TM oxides and the κ-type organic conductors belong to the same space group *Pnma*, which also supports the similarity; the C-AFM order here corresponds to the AFM structure in the κ-type organic system, both breaking the in-plane glide symmetry. We note that a similar mechanism without spin-orbit coupling was discussed for other materials [26–29]. Our work here illuminates spin current generation feasible in ubiquitous materials, based on a microscopic model calculation.

Finally, we discuss possible experimental detections of the present spin current generation in perovskites. One of the candidates is $CaCrO_3$, containing Cr^{4+} ions with the nominal $(3d)^2$ electron configuration, which shows the C-AFM metallic state below 90 K [39–41]. The Cr-O-Cr bond angle is 160°, which corresponds to the BX_6 rotation angle $\phi \approx 12^\circ$. According to a first-principles band calculation for $CaCrO_3$ [42], the on-site Coulomb interaction is deduced to be $U < 1.5$ eV, which is semiquantitatively consistent with our Hartree-Fock results, where the critical value of U at which the magnetic transition occurs is generally underestimated [43,44]. Within our model calculation, the spin-charge conversion ratio α is estimated up to around 0.5%. The C-AFM state is also observed in a series of vanadates AVO_3, with A=La–Y, which also have the $(3d)^2$ electron configuration and $\phi \approx 14^\circ$–22°, below around 100–150 K [45–48]. These values of ϕ correspond to $\alpha = 1\%$–4 % in our calculation. Although the C-AFM phases in these compounds are generally insulating due to the coexistence of the G-type OO, the carrier doping by substitution of the A ion reduces OO and stabilizes the metallic phase [49]. In addition, we note that the present mechanism works in a wide range of the electron filling once the C-AFM order is stabilized, as it is solely dictated by the symmetry. For example, we have found a similar spin splitting also in the d^4 system owing to the real-space anisotropies of the e_g-e_g and e_g-t_{2g} hopping integrals. Therefore, manganites $R_xA_{1-x}MnO_3$, which are known to show the C-AFM state [50–53], are also candidates.

The spin current generation presented here is not expected in the A- and G-type AFM phases, which are also widely seen in perovskite TM oxides in addition to the C-AFM phase. This is understood from the symmetry of the $GdFeO_3$-type distortion. Because of the mirror symmetry with respect to the ac plane, the anisotropies of the hopping integrals in the ac plane around B_1 and B_2 shown in Figs. 1(d) and 1(e) are equivalent to those around the B_3 and B_4 sites, respectively. Therefore, the AFM order with the same spins on the B_1 and B_3 sites and the opposite spins on the B_2 and B_4 sites, i.e., C-AFM, is essential for the nonzero spin current generation. In the A- and G-type AFM states, the spin currents cancel out.

The present calculation is based on the Hubbard model without the spin-orbit coupling, while, experimentally, it is expected that the conventional spin Hall effect appears due to the spin-orbit coupling of the TM ions, especially in 4d and 5d perovskites, in addition to the present mechanism [27]. Nevertheless, we can separate these two contributions, taking advantage of the difference between the symmetries of the spin current conductivity tensors as discussed in Ref. [25]; the conductivity tensor of the present mechanism is symmetric, while that of the spin Hall effect is antisymmetric, which makes

the different electric-field-angle dependences of the generated spin current. For example, in certain directions, e.g., the [101] direction, our mechanism gives a longitudinal response, whereas the spin Hall effect always provides the transverse one. The cooperative effect between the present mechanism and the spin-orbit coupling [54,55] is a future issue.

V. SUMMARY

In summary, we have shown that perovskites can serve as a spin current generator by applying an electric field, which originates from the cooperation of the $GdFeO_3$-type lattice distortion ubiquitously seen in a wide range of perovskites and *C*-type AFM ordering. We note that this mechanism is similar to the spin current generation in ferromagnet metals, while the net magnetization is absent in the AFM system. This enables us to generate a pure spin current without charge current, in contrast to the spin-polarized current in ferromagnets. It would be an interesting issue to study spin current generation by applying a thermal gradient to the *C*-AFM Mott insulating state. Here, the spatially anisotropic electron transfers lead to the anisotropic exchange interactions, which will give rise to a spin-dependent transport of the magnon, as demonstrated in Ref. [25].

ACKNOWLEDGMENTS

The authors would like to thank Y. Fuseya, T. Katsufuji, T. Mizokawa, M. Mochizuki, and I. V. Solovyev for valuable comments and discussions. This work is supported by Grants-in-Aid for Scientific Research No. JP19K03723, No. JP19K21860, and No. JP19H05825; JST-CREST (Grant No. JPMJCR18T2); and the GIMRT Program of the Institute for Materials Research, Tohoku University, Grant No. 19K0019.

[1] M. Imada, A. Fujimori, and Y. Tokura, Rev. Mod. Phys. **70**, 1039 (1998).
[2] S.-W. Cheong, Nat. Mater. **6**, 927 (2007).
[3] S. Maekawa, T. Tohyama, S. E. Barnes, S. Ishihara, W. Koshibae, and G. Khaliulin, *Physics of Transition Metal Oxides* (Springer, Berlin, 2004).
[4] R. J. D. Tilley, *Perovskites: Structure-Property Relationships* (Wiley, Chichester, UK, 2016).
[5] E. Wainer and A. N. Salomon, Titanium Alloy Mfg. Co. Elec. Rep. **8** (1942).
[6] J. B. Torrance, P. Lacorre, A. I. Nazzal, E. J. Ansaldo, and Ch. Niedermayer, Phys. Rev. B **45**, 8209 (1992).
[7] T. Kimura, T. Goto, H. Shintani, K. Ishizaka, T. Arima, and Y. Tokura, Nature (London) **426**, 55 (2003).
[8] M. A. Korotin, S. Yu. Ezhov, I. V. Solovyev, V. I. Anisimov, D. I. Khomskii, and G. A. Sawatzky, Phys. Rev. B **54**, 5309 (1996).
[9] J. G. Bednorz and K. A. Müller, Z. Phys. B **64**, 189 (1986).
[10] A. Kojima, K. Teshima, Y. Shirai, and T. Miyasaka, J. Am. Chem. Soc. **131**, 6050 (2009).
[11] M. N. Baibich, J. M. Broto, A. Fert, F. NguyenVan Dau, F. Petroff, P. Etienne, G. Creuzet, A. Friederich, and J. Chazelas, Phys. Rev. Lett. **61**, 2472 (1988).
[12] J. C. Slonczewski, J. Magn. Magn. Mater. **159**, L1 (1996).
[13] Y. Tserkovnyak, A. Brataas, and G. E. W. Bauer, Phys. Rev. Lett. **88**, 117601 (2002).
[14] K. Uchida, S. Takahashi, K. Harii, J. Ieda, W. Koshibae, K. Ando, S. Maekawa, and E. Saitoh, Nature (London) **455**, 778 (2008).
[15] I. Žutić, J. Fabian, and S. Das Sarma, Rev. Mod. Phys. **76**, 323 (2004).
[16] M. I. Dyakonov and V. I. Perel, ZhETF Pis. Red. **13**, 657 (1971) [JETP Lett. **13**, 467 (1971)].
[17] J. E. Hirsch, Phys. Rev. Lett. **83**, 1834 (1999).
[18] S. Murakami, N. Nagaosa, and S. C. Zhang, Science **301**, 1348 (2003).
[19] J. Sinova, D. Culcer, Q. Niu, N. A. Sinitsyn, T. Jungwirth, and A. H. MacDonald, Phys. Rev. Lett. **92**, 126603 (2004).
[20] Y. K. Kato, R. C. Mayers, A. C. Gossard, and D. D. Awschalom, Science **306**, 1910 (2004).
[21] J. Wunderlich, B. Kaestner, J. Sinova, and T. Jungwirth, Phys. Rev. Lett. **94**, 047204 (2005).
[22] E. Saitoh, M. Ueda, H. Miyajima, and G. Tatara, Appl. Phys. Lett. **88**, 182509 (2006).
[23] J. Železný, Y. Zhang, C. Felser, and B. Yan, Phys. Rev. Lett. **119**, 187204 (2017).
[24] M. Kimata, H. Chen, K. Kondou, S. Sugimoto, P. K. Muduli, M. Ikhlas, Y. Omori, T. Tomita, A. H. MacDonald, S. Nakatsuji, and Y. Otani, Nature (London) **565**, 627 (2019).
[25] M. Naka, S. Hayami, H. Kusunose, Y. Yanagi, Y. Motome, and H. Seo, Nat. Commun. **10**, 4305 (2019).
[26] S. Hayami, Y. Yanagi, and H. Kusunose, J. Phys. Soc. Jpn. **88**, 123702 (2019).
[27] R. González-Hernández, L. Šmejkal, K. Výborný, Y. Yahagi, J. Sinova, T. Jungwirth, and J. Železný, arXiv:2002.07073 [Phys. Rev. Lett. (to be published)].
[28] L.-D. Yuan, Z. Wang, J.-W. Luo, E. I. Rashba, and A. Zunger, Phys. Rev. B **102**, 014422 (2020).
[29] S. Hayami, Y. Yanagi, and H. Kusunose, Phys. Rev. B **102**, 144441 (2020).
[30] A. M. Glazer, Acta Crystallogr., Sect. B **28**, 3384 (1972).
[31] M. O'Keeffe and B. G. Hyde, Acta Crystallogr., Sect. B **33**, 3802 (1977).
[32] T. Mizokawa and A. Fujimori, Phys. Rev. B **54**, 5368 (1996).
[33] M. Mochizuki and M. Imada, J. Phys. Soc. Jpn. **70**, 1777 (2001).
[34] M. Mochizuki and M. Imada, J. Phys. Soc. Jpn. **71**, 2039 (2002).
[35] W. A. Harrison, *Electronic Structure and the Properties of Solids: The Physics of the Chemical Bond* (Freeman, San Francisco, 1980)
[36] E. Pavarini, S. Biermann, A. Poteryaev, A. I. Lichtenstein, A. Georges, and O. K. Andersen, Phys. Rev. Lett. **92**, 176403 (2004).
[37] S. Sugano, Y. Tanabe, and H. Kamimura, *Multiplets of Transition-Metal Ions in Crystals* (Academic, New York, 1970).
[38] Y. Wang, P. Deorani, X. Qiu, J. H. Kwon, and H. Yang, Appl. Phys. Lett. **105**, 152412 (2014).

[39] A. C. Komarek, S. V. Streltsov, M. Isobe, T. Möller, M. Hoelzel, A. Senyshyn, D. Trots, M. T. Fernández-Díaz, T. Hansen, H. Gotou, T. Yagi, Y. Ueda, V. I. Anisimov, M. Grüninger, D. I. Khomskii, and M. Braden, Phys. Rev. Lett. **101**, 167204 (2008).
[40] P. A. Bhobe, A. Chainani, M. Taguchi, R. Eguchi, M. Matsunami, T. Ohtsuki, K. Ishizaka, M. Okawa, M. Oura, Y. Senba, H. Ohashi, M. Isobe, Y. Ueda, and S. Shin, Phys. Rev. B **83**, 165132 (2011).
[41] S. V. Streltsov, M. A. Korotin, V. I. Anisimov, and D. I. Khomskii, Phys. Rev. B **78**, 054425 (2008).
[42] H. M. Liu, C. Zhu, C. Y. Ma, S. Dong, and J.-M. Liu, J. Appl. Phys. **110**, 073701 (2011).
[43] M. J. Rozenberg, G. Kotliar, H. Kajueter, G. A. Thomas, D. H. Rapkine, J. M. Honig, and P. Metcalf, Phys. Rev. Lett. **75**, 105 (1995).
[44] Z. H. Zhu, F. J. Rueckert, J. I. Budnick, W. A. Hines, M. Jain, H. Zhang, and B. O. Wells, Phys. Rev. B **87**, 195129 (2013).
[45] V. G. Zubkov, G. V. Bazuev, V. A. Perelyaev, and G. P. Shveikin, Sov. Phys. Solid State **15**, 1079 (1973).
[46] H. Sawada, N. Hamada, K. Terakura, and T. Asada, Phys. Rev. B **53**, 12742 (1996).
[47] S. Miyasaka, Y. Okimoto, M. Iwama, and Y. Tokura, Phys. Rev. B **68**, 100406(R) (2003).
[48] Y. Motome, H. Seo, Z. Fang, and N. Nagaosa, Phys. Rev. Lett. **90**, 146602 (2003).
[49] S. Miyasaka, T. Okuda, and Y. Tokura, Phys. Rev. Lett. **85**, 5388 (2000).
[50] Y. Tokura and Y. Tomioka, J. Magn. Magn. Mater. **200**, 1 (1999).
[51] E. Dagotto, T. Hotta, and A. Moreo, Phys. Rep. **344**, 1 (2001).
[52] R. Kajimoto, H. Yoshizawa, Y. Tomioka, and Y. Tokura, Phys. Rev. B **66**, 180402(R) (2002).
[53] I. V. Solovyev, Phys. Rev. B **55**, 8060 (1997).
[54] M. Naka, S. Hayami, H. Kusunose, Y. Yanagi, Y. Motome, and H. Seo, Phys. Rev. B **102**, 075112 (2020).
[55] L. Šmejkal, R. González-Hernández, T. Jungwirth, and J. Sinova, Sci. Adv. **6**, eaaz8809 (2020).